Trajectory options for Hera's Milani CubeSat around (65803) Didymos

Fabio Ferrari · Vittorio Franzese · Mattia Pugliatti · Carmine Giordano · Francesco Topputo

Received: date / Accepted: date

Abstract The dynamical environment in the close-proximity of small celestial bodies is characterized by a very weak and irregular gravity field. In this low-acceleration deep-space environment, small dynamical perturbations might affect significantly the dynamics of a spacecraft hovering near the surface of such objects. This poses a challenge to the efficient design of trajectories of space probes for space missions aimed at the exploration of small Solar System bodies. This applies especially to CubeSats, small spacecraft with limited autonomy and maneuvering capabilities. In this case, a careful and efficient design of the operational trajectory is mandatory to accomplish the objective of the mission. As a representative and timely case study, we investigate the dynamics around binary asteroid (65803) Didymos, the target of NASA's Double Asteroid Redirection Test (DART) and ESA's Hera missions. We analyze all the relevant dynamical contributions concurring to the acceleration environment near Didymos and provide a subdivision of it into subregions, each identified by a different dynamical regime. With reference to the Hera Milani CubeSat mission scenario, we describe the methodology and design approach to find trajectories in the dayside of Didymos system. Finally, we provide examples of suitable trajectory options to host the operational phase of the Hera Milani CubeSat.

Keywords Hera · Milani · asteroid · CubeSat · Didymos · binary

F. Ferrari, V. Franzese, M. Pugliatti, C. Giordano, F. Topputo
Politecnico di Milano, Department of Aerospace Science and Technology
Via La Masa 34, 20156, Milan, Italy
Tel.: +39 02-2399-8308
E-mail: fabio1.ferrari@polimi.it

1 Introduction

In the past few decades, small celestial bodies in our Solar System have been chosen as targets of several space exploration missions. In particular, the accessibility of Near Earth Asteroids (NEAs) provides insightful scientific and technological opportunities for medium/low-cost missions. In this context, it is crucial to address the challenges of such low-gravity, deep-space environments. The understanding of the dynamics in the close-proximity of these objects can help maximizing the scientific and technological return of the missions. This is the case when low-cost platforms, such as CubeSats and SmallSats, are used. These have limited on-board resources and maneuvering capabilities, and thus benefit greatly from a careful design and mission profile planning.

In this work, we study the dynamical environment near (65803) Didymos, the NEA binary asteroid targeted by the Asteroid Impact and Deflection Assessment (AIDA), the first planetary defense mission: an international collaboration between NASA and ESA (Cheng et al, 2015). In this context, the secondary asteroid of Didymos (called Dimorphos) will be impacted by NASA's Double Asteroid Redirection Test (DART) spacecraft (Cheng et al, 2018) in 2022. Before impact, DART will release LICIACube (Tortora and Tana, 2019; Cheng et al, 2020), a CubeSat that will fly by Didymos and leave the system shortly after DART's impact. The binary system will be visited again in 2027, by ESA's Hera mission (Michel et al, 2018). Hera will rendezvous with Didymos and carry out scientific investigation on the dynamical and physical properties of the binary system. To support scientific operations, Hera will release two 6U CubeSats in the close proximity of Didymos: Juventas (Karatekin et al, 2019) and Milani (Ferrari et al, 2021). These will be the first interplanetary CubeSat to execute long-term operations in the close proximity of a binary asteroid system, benefiting from 6-DOF maneuver capabilities.

Recent studies address the problem of the binary relative dynamics between Didymos (primary) and Dimorphos (secondary) (Agrusa et al, 2020), using a high-fidelity shape modeling of asteroids and mutual gravity between them (Hou et al, 2016; Davis and Scheeres, 2020; Yu et al, 2019). In our work instead, we focus on the dynamical environment near the binary system: the motion of asteroids is prescribed and not solved. In this context, general studies have analyzed the long-term natural dynamics of dust (Yu and Michel, 2018) as well as the stability and feasibility of orbital motion in the vicinity of Didymos binary system (Dell'Elce et al, 2017; Lasagni Manghi et al, 2018; Capannolo et al, 2019), and in its very close proximity (Ferrari and Lavagna, 2018). These studies show that the dynamical environment near binary asteroid systems is extremely chaotic, and confirm the results of similar investigations in small-body environments (Ferrari et al, 2016; Tardivel, 2016; Van Wal et al, 2017; Damme et al, 2017; Soldini et al, 2020; Villegas-Pinto et al, 2020). In such low-acceleration environment, the effect of Solar Radiation Pressure (SRP) is extremely relevant and plays a fundamental role in driving the motion of a lightweight spacecraft (Guzzetti et al, 2019; Jean et al, 2019).

Table 1: Physical and dynamical properties of Didymos binary system; shape-based models of asteroids used in this work.

Parameter	Didymos (D1)	Dimorphos (D2)
Mass	5.2294e11 kg	4.8633e9 kg
Bulk density	2170 kg/m^3	2170 kg/m^3
Spinning period	2.26 h	11.92 h
Shape	Polyhedron (radar model by Naidu et al (2020))	Triaxial ellipsoid (α, β, γ)= (103, 79, 66) m

The goal of the paper is to develop a high-fidelity model of the dynamical environment near Didymos binary and investigate suitable trajectory options to host a CubeSat, with application to Hera's Milani. More in detail, after introducing the properties of Didymos (Section 1.1), we present in Section 2 the formalization of the equations that govern the motion of a CubeSat in the proximity of Didymos, considering all relevant perturbations and a high-fidelity representation of the asteroids' gravity field. In the same section we provide a subdivision of the dynamical environment according to relevant effects governing the dynamics of the CubeSat. Section 3 discusses the strategy adopted for trajectory design, and Section 4 presents suitable trajectory options. We then investigate trajectory options for the Milani CubeSat mission scenario. The main results and conclusion are eventually summarized in Section 5.

1.1 Didymos properties

We report here figures and assumptions relevant to the modelling of the dynamical environment near the binary asteroid. In particular, a summary of relevant parameters used is provided in Table 1. These are consistent with up-to-date estimated ranges reported by Naidu et al (2020). The dynamical and orbital properties of the Didymos barycenter and asteroid objects Didymos (also referenced as D1 or primary in the followings) and Dimorphos (also D2 or secondary) are retrieved from the up-to-date orbital kernels of the Hera mission study[1].

In terms of relative orientation, we assume that the spin vector of Didymos is aligned to the angular momentum vector of Dimorphos orbit around the primary. Also, the secondary is currently assumed to be in a tidally-locked configuration: therefore, its spin period is synchronized with its revolution period around Didymos. In this configuration, the binary relative motion occur on the equatorial plane of D1, which is also the equatorial plane of D2. Note that the relative motion within the Didymos binary system is retrograde as the Didymos equatorial plane is nearly flipped upside down with respect to

[1] https://www.cosmos.esa.int/web/spice/data, Version: 081, Last accessed: December 2020.

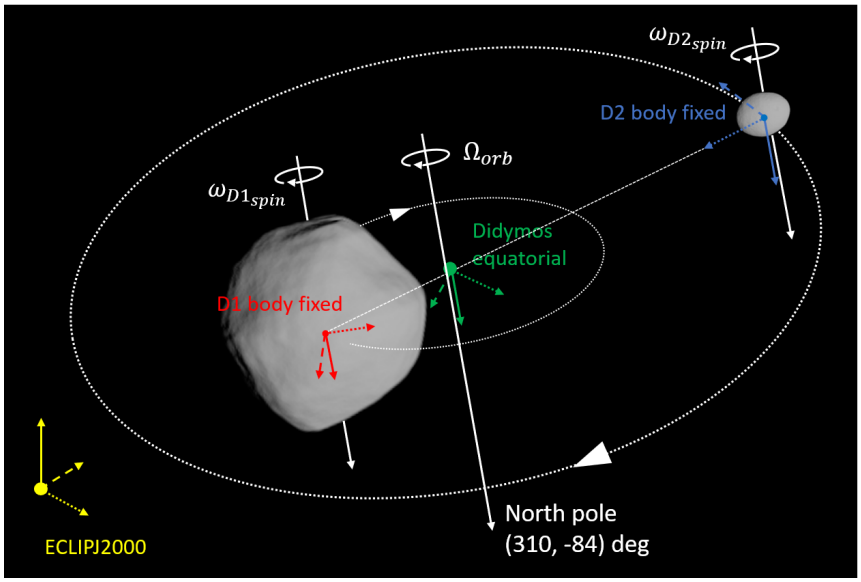

Fig. 1: Geometry of the Didymos system. Reference frames used in this work are highlighted. The red and blue triads are the Didymos and Dimorphos body-fixed reference frames, respectively. The yellow triad is the ECLIPJ2000 reference frame (also called DidymosECLIPJ2000 when centered in the Didymos system barycenter). The dotted, dashed, and continuous lines represent the x, y, and z axis of each reference frame, respectively. The north pole direction is nearly flipped upside down with respect to the ecliptic plane. All spin and orbital motion within the binary are directed towards the north pole of the system.

the ecliptic plane, having ecliptic coordinates (λ, β)=(310,-84) deg (Scheirich and Pravec, 2009).

The shape of Didymos primary is modelled as a polyhedron using the radar model by Naidu et al (2020). The shape of Dimorphos is modelled using a triaxial ellipsoid, with axes as reported in Table 1. In its tidally-locked configuration, the greater (α) semi-axis of Dimorphos is aligned at any time to the D1–D2 direction, while the smaller axis (γ) is aligned to Dimorphos' spin vector, in the south–north pole direction. A schematic representation of the geometrical and dynamical features of Didymos is shown in Figure 1. The reference frames used in this work are also shown.

In this work, we consider the extended timeframe of the Hera/Milani mission, between 01-Jan-2027 and 01-Jan-2028. Figure 2a shows the heliocentric orbit of Didymos in the ECLIPJ2000 frame and Figure 2b shows the distance from the Sun in this timeframe. As shown in Figure 2, Hera is planned to arrive at Didymos in early 2027, when the asteroid is nearly at its perihelion.

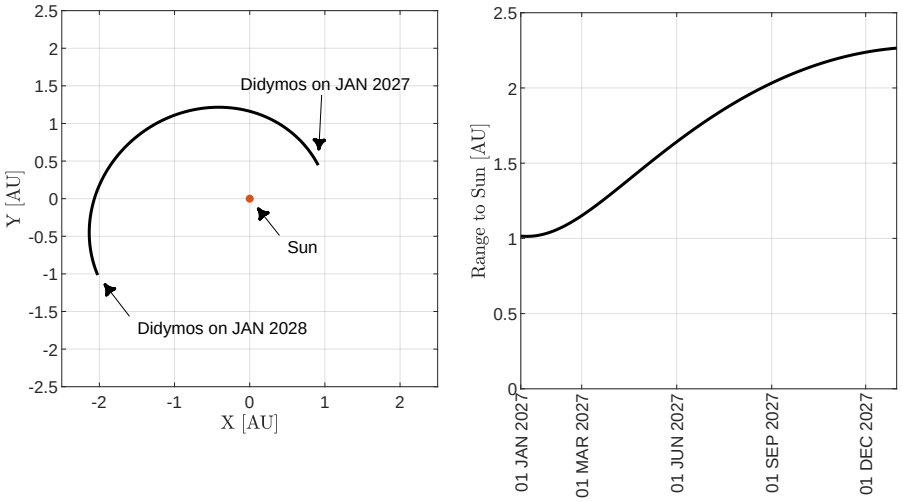

(a) (b)

Fig. 2: Didymos heliocentric motion in the interval between 01-Jan-2027 and 01-Jan-2028: (a) orbit in the ECLIPJ2000 frame and (b) distance from the Sun.

The distance from the Sun quickly increases as Didymos orbits towards its aphelion.

2 Dynamical environment

We discuss here the modelling of the dynamical environment near Didymos and formalize the equations that drive the dynamics of a CubeSat in the proximity of the binary asteroid. In the second part of this chapter, we discuss the subdivision of the region near Didymos into sub-regions, and the dynamical effects that govern each sub-region.

2.1 Equations of motion

To investigate the relative dynamics of the CubeSat near Didymos, we use a quasi-inertial reference frame, also later referenced as DidymosECLIPJ2000. This is centered at the barycenter of the binary system, which moves along Didymos heliocentric path, and therefore is not inertial. The axes (X,Y,Z) are intertially fixed, with X and Y lying on the ecliptic plane at epoch J2000, and Z orthogonal to this plane. We use the prefix *quasi* to highlight that the system can be considered inertial for characteristic times shorter than those related to Didymos heliocentric motion, which is typically the case of spacecraft orbit

design. This is a convenient choice, allowing the study of the Cubesat's relative motion with respect to the Didymos system.

As shown in the schematic provided in Figure 3, the dynamics of the CubeSat are driven by four main accelerations: the gravity of Didymos, $\boldsymbol{a}_{D_1}$, the gravity of Dimorphos, $\boldsymbol{a}_{D_2}$, the third-body effect of the Sun, $\boldsymbol{a}_{3b_S}$, and the Solar Radiation Pressure, $\boldsymbol{a}_{SRP}$. More detail on the importance of each contribution is provided in the next section. The position of Didymos, Dimorphos, and the Sun is resolved precisely, as provided by high-order integration in ESA's Hera Mission kernels. In their most general form, the equations of motion for a point mass (i.e., the CubeSat) in the proximity of Didymos system read

$$\ddot{\boldsymbol{r}} = \boldsymbol{a}_{D_1} + \boldsymbol{a}_{D_2} + \boldsymbol{a}_{3b_S} + \boldsymbol{a}_{SRP} \tag{1}$$

The acceleration $\boldsymbol{a}_{D_1}$ is due to the gravity of Didymos. As mentioned, the primary is a diamond-shaped asteroid, with an equatorial bulge and flattened poles (Naidu et al, 2020). The gravity field in the asteroid close-proximity can be best modelled by using its polyhedral shape model. In particular, we modelled the exterior field by computing the gravitational potential of a constant density polyhedron, using Didymos polyhedral shape model (Werner, 1994; Werner and Scheeres, 1997), as

$$\check{\boldsymbol{a}}_{D_1} = G\rho\left(\sum_{f \in \text{faces}} \mathbf{F}_f \cdot \check{\boldsymbol{r}}_f \omega_f - \sum_{e \in \text{edges}} \mathbf{E}_e \cdot \check{\boldsymbol{r}}_e L_e \right) \tag{2}$$

where G is the universal gravitational constant, ρ is the density of the polyhedron, $\check{\boldsymbol{r}}_f$ and $\check{\boldsymbol{r}}_e$ are vectors from the field point to face f and edge e, respectively. $\mathbf{F}_f$ is the dyad associated to face f and $\mathbf{E}_e$ is the dyad associated to edge e of the polyhedron model. ω_f is the solid angle associated to face f and L_e is the potential of a wire associated to edge e. Vectors $\check{\boldsymbol{a}}_{D_1}$, $\check{\boldsymbol{r}}_f$, and $\check{\boldsymbol{r}}_e$ in Eq. (2) are expressed in the asteroid body-fixed frame (see reference frames in Figure 1) and require a further transformation to be included into Eq. (1), that is

$$\boldsymbol{a}_{D_1} = \check{\mathbf{R}}\check{\boldsymbol{a}}_{D_1} \tag{3}$$

$$\boldsymbol{r}_f = \check{\mathbf{R}}\check{\boldsymbol{r}}_f + \boldsymbol{d}_{D_1} \tag{4}$$

$$\boldsymbol{r}_e = \check{\mathbf{R}}\check{\boldsymbol{r}}_e + \boldsymbol{d}_{D_1} \tag{5}$$

where $\check{\mathbf{R}}$ maps the rotation between Didymos body-fixed frame and the DidymosECLIPJ2000 frame, while $\boldsymbol{d}_{D_1}$ is the position of D1 in the latter frame.

The gravitational contribution of Dimorphos is computed using the potential of a uniform-density, tri-axial ellipsoid (Scheeres, 1994). The acceleration field is derived accordingly as

$$\tilde{\boldsymbol{a}}_{D_2} = -2G\rho\pi\alpha\beta\gamma \begin{Bmatrix} \tilde{x} \int_\lambda^\infty \frac{du}{(\alpha^2+u)\Delta(u)} \\ \tilde{y} \int_\lambda^\infty \frac{du}{(\beta^2+u)\Delta(u)} \\ \tilde{z} \int_\lambda^\infty \frac{du}{(\gamma^2+u)\Delta(u)} \end{Bmatrix} \tag{6}$$

with

$$\Delta(u) = \sqrt{(\alpha^2+u)(\beta^2+u)(\gamma^2+u)} \tag{7}$$

where α, β, γ, are the semi-axes of the ellipsoid (with $\alpha \geq \beta \geq \gamma$), and $(\tilde{x}, \tilde{y}, \tilde{z})$ are the components of the field point vector $\tilde{\boldsymbol{r}}_{ell}$, representing the distance from the ellipsoid. Equation (6) is expressed in the Dimorphos body-fixed frame, with its axes aligned to the principal axes of inertia of the ellipsoid. The following transformation is required to include the acceleration field $\tilde{\boldsymbol{a}}_{D_2}$ into Eq. (1):

$$\boldsymbol{a}_{D_2} = \tilde{\mathbf{R}}\tilde{\boldsymbol{a}}_{D_2} \tag{8}$$

$$\boldsymbol{r}_e = \tilde{\mathbf{R}}\tilde{\boldsymbol{r}}_e + \boldsymbol{d}_{D_2} \tag{9}$$

where $\tilde{\mathbf{R}}$ maps the rotation between Dimorphos body-fixed frame and the DidymosECLIPJ2000 frame, while $\boldsymbol{d}_{D_2}$ is the position of the secondary in the latter frame. Rotation matrices $\check{\mathbf{R}}$ and $\tilde{\mathbf{R}}$ evolve in time, and are computed based on the precise position and orientation of D1 and D2, as retrieved from their ephemerides.

The third-body effect of the Sun in Eq. (1) is written in the Didymos barycenter, which in turn orbits the Sun. That is, $\boldsymbol{a}_{3b_S}$ models the Keplerian gravity gradient between the barycenter of Didymos system and the field point:

$$\boldsymbol{a}_{3b_S} = (\mu_S + \mu_D)\frac{\boldsymbol{r}_{D-S}}{\|\boldsymbol{r}_{D-S}\|^3} - \mu_S \frac{\boldsymbol{r}_{C-S}}{\|\boldsymbol{r}_{C-S}\|^3} \tag{10}$$

where $\mu_S = Gm_S$ and $\mu_D = G(m_{D_1} + m_{D_2})$ are the gravitational constants of the Sun and Didymos system, respectively, $\boldsymbol{r}_{D-S}$ and $\boldsymbol{r}_{C-S}$ are the position vectors of Didymos system barycenter and the field point with respect to the Sun, in the DidymosECLIPJ2000 reference frame, with reference to Figure 1 and 3. The relative position between Didymos system barycenter and the Sun is retrieved at each epoch from the ephemerides data. Note that in our case $\mu_D << \mu_S$, and thus Eq. (10) can be simplified to:

$$\boldsymbol{a}_{3b_S} \simeq \mu_S \left(\frac{\boldsymbol{r}_{D-S}}{\|\boldsymbol{r}_{D-S}\|^3} - \frac{\boldsymbol{r}_{C-S}}{\|\boldsymbol{r}_{C-S}\|^3} \right) \tag{11}$$

The last contribution of Eq. (1) is due to Solar Radiation Pressure (SRP) that pushes the CubeSat away from the Sun. This contribution is computed using a SRP cannonball model (Chobotov, 1991):

$$\boldsymbol{a}_{SRP} = \frac{P_0}{c}\left(\frac{D_{AU}}{\|\boldsymbol{r}_{C-S}\|}\right)^2 \frac{C_r A}{M}\hat{\boldsymbol{r}}_{C-S} \tag{12}$$

where P_0 (1367 W/m^2) is the solar flux at 1 AU, c is the speed of light (2.998×10^8 m/s), D_{AU} is the Sun–Earth distance (1 AU = 1.495×10^{11} m), C_r is the reflectivity coefficient of the CubeSat, A is its equivalent surface area, and M is its mass.

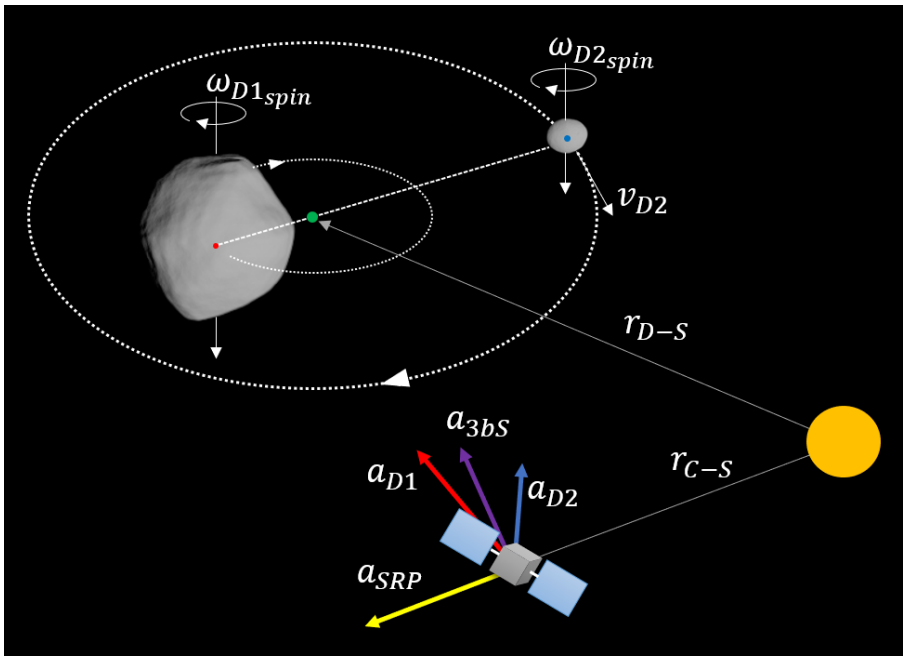

Fig. 3: Schematic of the contributions of the acceleration field on the CubeSat.

2.2 Dynamical regimes

The complex environment near Didymos can be subdivided into regions, where the motion of the CubeSat is dominated by different dynamical regimes. The four dynamical effects concurring to the right-hand side of Eq. (1) (gravity of D1, gravity of D2, third-body gravitational effect of the Sun and SRP) are analyzed into detail and their relevance to the motion of a CubeSat is assessed.

Figure 4 shows the accelerations acting on a field point as function of its distance from Didymos barycenter. The acceleration due to SRP is computed for the Milani CubeSat case, while all other effects are independent from the spacecraft mass. Acceleration ranges are shown in the time interval between 01-Jan-2027 and 01-Jan-2028, which is relevant for Milani. In particular, the effect of SRP and third-body gravity of the Sun depends on the Didymos–Sun distance and are maximum when the asteroid is closer to its pericenter (beginning of 2027, as shown in Figure 2). Instead, the range variation in D1 and D2 gravity depends on the position of the asteroids with respect to the barycenter of the Didymos system, with a characteristic time of nearly 12 h. Values shown in Figure 4 are computed for distances ranging between the average radius of Didymos primary (390m) and 40 km from Didymos barycenter. The orbital region of Dimorphos (orbital semimajor axis $\pm$ mean radius of D2) is shadowed in grey. As expected, Figure 4 shows that near Didymos, the gravity of the asteroids, and D1 in particular, dominates over

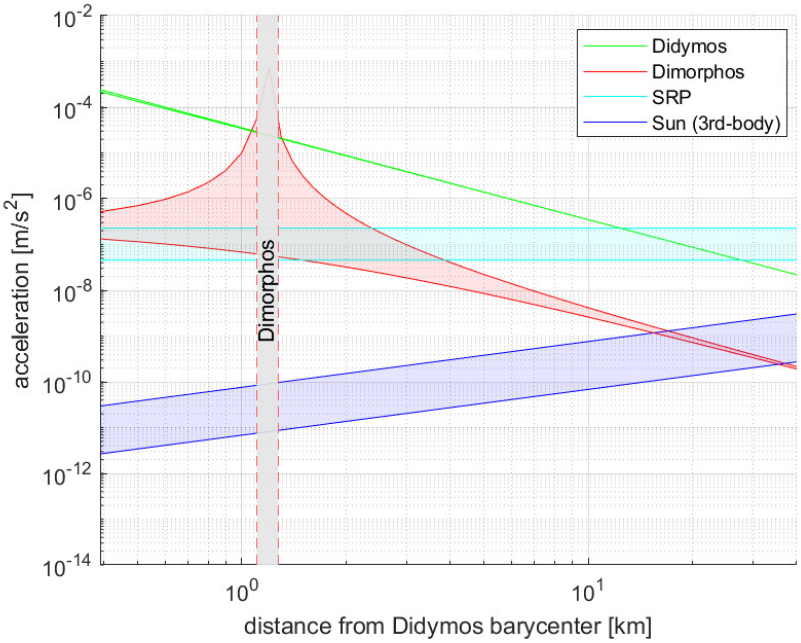

Fig. 4: Main accelerations in the proximity of Didymos binary system. Gravity of Didymos (primary) and Dimorphos, Sun (third body) and Solar Radiation Pressure (SRP) as function of the distance from the barycenter of Didymos system are highlighted. Ranges between minimum and maximum values in the interval 01-Jan-2027 and 01-Jan-2028 are shown as shadowed region.

SRP and third-body effect of the Sun. Farther away the dynamics are gradually taken over by the SRP, which becomes the most relevant effect at about >10 km, and ultimately by the Keplerian shift due to Sun's third-body effect, which dominates the dynamics at >1,000 km away from Didymos.

Figure 5 gives further insights, by comparing the acceleration provided by different models of the dynamics in the proximity of Didymos system. In particular, the results from eight different models have been compared, each reproducing the dynamical environment to a different level of detail. Four main model subsets are studied:

- All four effects considered: gravity of D1, gravity of D2, third-body gravity of the Sun, SRP (red curves in Figure 5)
- Gravity of the D1 and D2 only (cyan)
- Gravity of D1 only (blue)
- Gravity of D2 only (green)

Also, each of these subset is implemented using two different models for asteroids' gravity: either shape-based models (solid lines and marked with prefix "s" in the legend of Figure 5) or simpler point-mass central fields (dashed

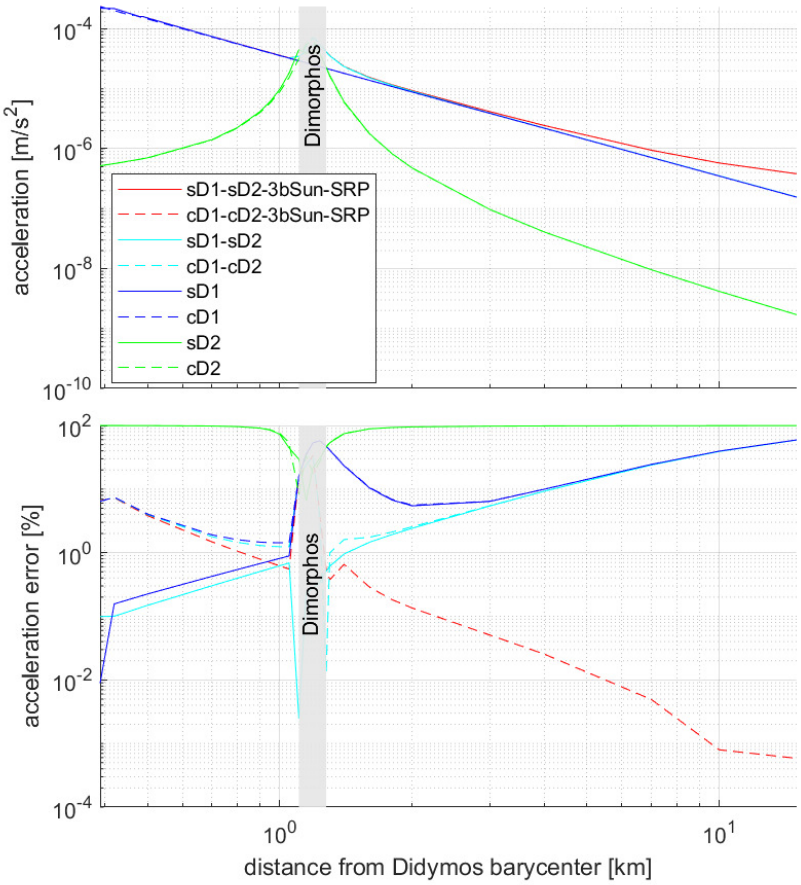

Fig. 5: Comparison between different models of the dynamics near Didymos system. Absolute accelerations are shown in the upper plot. Relative errors with respect to the high-fidelity model (sD1-sD2-3bSun-SRP) are shown in the lower plot. Different models combine the effects of shape-based gravity models of asteroids (marked with prefix "s", solid lines) versus central-field models ("c", dashed lines). The third-body effect of the Sun (3bSun) and SRP are also considered.

lines, prefix "c"). We call "high-fidelity model" the one that considers all four effects and asteroids shape-based models ("sD1-sD2-3bSun-SRP" in Figure 5). Since this model is the most accurate and detailed available, we use this as a real-world reference: other models are simplifications of the high-fidelity one. The comparison between simplified and high-fidelity models provides insightful information about the predominance of dynamical effects near Didymos system. The upper part of Figure 5) shows the acceleration field computed by

Table 2: Dynamical regions near Didymos system. Ranges in terms of distance from the barycenter of Didymos binary.

	Range	Relevant effects	Main effect
Inner	<1.1 km	D1 (shape) + D2 (point mass) + SRP	D1
region	1.1-1.3 km	D1 (point mass) + D2 (shape) + SRP	D2
Mid-range	1.3-4 km	D1 (point mass) + D2 (point mass) + SRP	D1
region	4-10 km	D1+D2 (single point mass) + SRP	D1
Outer	10-1000 km	D1+D2 (single point mass) + SRP + 3bSun	SRP
region	>1000 km	SRP + 3bSun	3bSun

each model, whereas the lower part shows the relative error (in percentage) between accelerations magnitudes computed in the simplified model (a) versus the high-fidelity one (a_{HiFi}). This is computed as:

$$a_{\mathrm{err}} = \frac{a - a_{\mathrm{HiFi}}}{a_{\mathrm{HiFi}}} \times 100 \qquad [\%] \tag{13}$$

As expected, Figure 5 shows that higher-fidelity models of asteroids (shape-based models) are required when the CubeSat flies close to them. In particular, the shape model of D1 shall be used to keep a relative error of 1% or less at a distance <800 m from Didymos barycenter (about 400 m from the surface of D1). Farther away, a simpler central field can be employed for D1. Similarly, the shape model of D2 should be used close to it, in the range 1.1-1.3 km from Didymos barycenter (up to 50 m from the surface of D2). In these very-close-proximity regions, SRP might be neglected for very short trajectory arcs (Ferrari and Lavagna, 2018). However, it quickly becomes very relevant as the distance from the system increases and cannot be disregarded at distances >800 m from the system.

As a result, the environment in the proximity of Didymos can be subdivided into regions, as summarized in Table 2. We identify with the term *inner region* the region nearly within the orbital radius of D2 around the barycenter of Didymos (<1.3 km). As mentioned, the dynamics within this region are dominated by the gravity of the asteroids. Perturbations due to the non-spherical shape of asteroids become relevant. In this case, an accurate modelling of their gravitational dynamics would benefit from the representation of such perturbation, using, e.g., shape-based representation of the asteroids, or spherical harmonics. As mentioned, in our work we use shape-based models rather than a potential series method because of their better accuracy near the surface of the asteroids (Scheeres, 2016). A shape-based model shall be used within a distance of about 400 m from the surface of D1 and about 50 m from the surface of D2.

We call *mid-range* the region between 1.3 km and 10 km. As for the inner region, the main acceleration is due to the gravity of D1, but SRP is nearly on the same order of magnitude and can never be neglected. For distances >4 km, the gravity due to the two asteroids can be summed up and modelled as a single

point-mass at the barycenter of Didymos system with little error. This can be inferred qualitatively from Figure 5, with errors of D1 and D1-D2 models becoming equal above 4 km. The separate effects of the two asteroids are felt at shorter ranges (<4 km), where the CubeSat dynamics follow a restricted three-body gravitational problem (R3BP), rather than a simpler R2BP. Note that the gravity field of the secondary can be measured indirectly from greater distances as well: e.g., Zannoni et al (2018) report that the mass of Dimorphos can be estimated through radio science from a distance of 10 km. However, the subdivision proposed here is made for trajectory design purposes only, to reproduce the dynamical environment and not to assess its observational limits.

In the *outer region* (>10 km from the barycenter of Didymos binary) the gravitational pull of Didymos system becomes weak and the dynamics are dominated by SRP and/or third-body effect of the Sun. The Keplerian shear due to the heliocentric motion of Didymos (third-body effect of the Sun) plays a significant role as the distance increases. It overcomes the gravity of Didymos for distances greater than 100 km and overcomes the SRP above 1000 km, where the dynamics follow a pure Keplerian drift between the heliocentric orbits of Didymos system and the CubeSat.

3 Trajectory design approach

This section presents the design approach and numerical methods used to find trajectories suitable for a CubeSat mission in the vicinity of Didymos. In particular, considering the subdivision of dynamical regions discussed in Section 2.2, we identify two main design approaches. We discuss here the suitability of each approach in terms of dynamical constraints of the mission. Sample trajectory solutions obtained are then reported in Section 4.

(a) *Stable orbit.* A convenient strategy to operate a CubeSat makes use of stable orbits. This has the advantage of requiring low operational and maintenance effort in terms of maneuvering. Also, the Δv required is typically very limited. However, the environment near Didymos is extremely chaotic and it is hard to find long-term stable motion. In particular, in the external region (>4 km) the motion is heavily affected by the SRP, which pushes steadily the CubeSat towards the anti-Sun direction. This results in a secular variation of the CubeSat orbit, which is hardly compatible with natural periodic motion. Therefore, no long-term stable motion exists in the external region. A natural stabilizing effect can be enforced by exploiting the gravitational attraction of asteroids. This can be achieved closer to the binary system (<4 km), when the gravitational pull of asteroids overcomes the effect of SRP. In particular, relative stable motion can be found by exploiting three-body solutions: these include orbits about libration points (e.g., L4 and L5), as well as Didymos- and Dimorphos-centered orbits. Another option is the one employed by the Juventas CubeSat, which plans to fly a Self-Stabilized Terminator Orbit (SSTO) around the binary

system, at a distance in the range 2-5 km from the barycenter of Didymos (Goldberg et al, 2019). The geometry of the terminator orbit provides a stabilizing balance between the gravitational pull of the asteroids and the steadily push of SRP. The drawback of this approach is the limited flexibility in terms of range and illumination conditions achievable from the terminator, e.g., the phase angle CubeSat-asteroid-Sun will always be kept at around 90 deg. This is not an issue in case of active payloads (as for Juventas, which carries a miniaturized radar), but might not be suitable to host passive payloads, such as multispectral imagers (as for the case of Milani).

(b) *Waypoint strategy.* As mentioned, stable motion is a suitable option only in the inner most region of the binary system and for very specific relative geometries (e.g., terminator). Apart from these limited cases, stable motion is not achievable due to the effect of SRP. When these cases are not applicable, a different strategy must be adopted. The *waypoint strategy* is a flexible strategy to operate a spacecraft, based on the selection of waypoints, which act as maneuver points between patched ballistic arcs. An example of a similar strategy in a small-body environment is found in pyramid-like orbits flown by the Rosetta spacecraft around comet 67P/Churyumov-Gerasimenko (Accomazzo et al, 2015). The geometrical configuration of waypoints is usually selected to meet mission constraints and grants high flexibility in terms of distance ranges, illumination conditions and relative geometry (phase angles). In the case of an asteroid exploration mission, the waypoints are typically selected to ensure that the CubeSat is always on the day side of the asteroids, such that they are constantly illuminated and visible on optical cameras. The drawback of this approach is the relatively high cost in terms of Δv (which however might not be an issue in low-accelerations/low-velocity small-body environments) and the high operational burden required. In fact, compared to the stable orbit case, the CubeSat requires maneuvers with a higher frequency (at waypoints after each ballistic arc).

Previous works investigate stable motion near Didymos system (Dell'Elce et al, 2017; Lasagni Manghi et al, 2018; Perez et al, 2018; Capannolo et al, 2019) or studied the close-proximity environment to design safe landing trajectories (Ferrari and Lavagna, 2018; Tardivel, 2016; Van Wal et al, 2017). On the other hand, none addresses the problem of spacecraft dynamics in the external region, i.e., where the dynamics is dominated by SRP. We address this problem here, using the waypoint strategy to find suitable trajectories. The waypoint strategy is well suited to the Milani case (Ferrari et al, 2021), as the scientific operations of the CubeSat require high flexibility in terms of distance range and phase angles to host observations with the hyperspectral camera ASPECT (Kohout et al, 2018). A detailed description of the waypoint-based design method, including numerical tools used, is discussed here below. Trajectory examples and analyses performed on the Didymos case study are reported in Section 4.

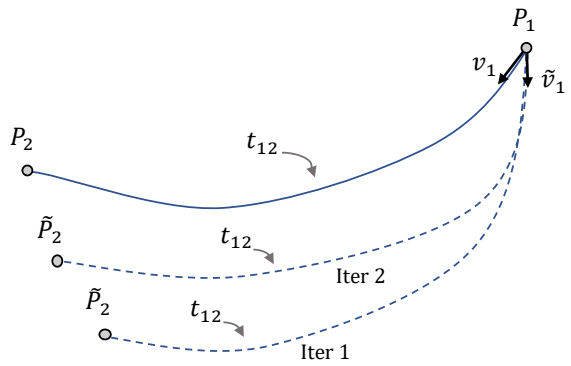

Fig. 6: Schematic of the iterative correction process. The initial guess on velocity $\tilde{\boldsymbol{v}}_1$ is used to propagate the dynamics forward for t_{12} time. Information on $\tilde{\boldsymbol{P}}_2$ is used to correct the initial guess in an iterative process, until the final position $\tilde{\boldsymbol{r}}_2$ matches with the position $\boldsymbol{r}_2$ at final waypoint $\boldsymbol{P}_2$, within an error ε ($\|(\boldsymbol{r}_2 - \tilde{\boldsymbol{r}}_2)\| < \varepsilon$).

3.1 Numerical method

Trajectories designed using a waypoint strategy consist of ballistic arcs patched together at maneuver points, called waypoints. The design of the ballistic arc between two consecutive waypoints is based on a step-wise differential correction procedure, and is the result of an iterative targeting problem. The step-wise elements are described as follows.

(i) *Initial conditions.* These are selected by the designer. They include the position of the waypoints $\boldsymbol{P}_1$ and $\boldsymbol{P}_2$) (labelled $\boldsymbol{r}_1$ and $\boldsymbol{r}_2$ in the following), the initial epoch t_1, and the time of flight between the waypoints t_{12}. These setting define the ballistic arc flowing from $\boldsymbol{P}_1$ to $\boldsymbol{P}_2$, which is to be found.

(ii) *Initial guess.* It is a guess on the initial velocity $\tilde{\boldsymbol{v}}_1$ at $\boldsymbol{P}_1$. It is desirable that $\tilde{\boldsymbol{v}}_1$ is close to the actual velocity $\boldsymbol{v}_1$ required to reach $\boldsymbol{P}_2$ after t_{12}. In this work, we use a Restricted Two-Body Problem (R2BP) Lambert's solver to find a suitable first guess. This method produces a initial solution neglecting the third-body perturbation and SRP, yet it guarantees convergence in few iterations to the target point $\boldsymbol{P}_2$ in most of the cases experimented.

(iii) *Correction.* The initial guess state $\tilde{\boldsymbol{x}}_1 = (\boldsymbol{r}_1; \tilde{\boldsymbol{v}}_1)$ is propagated forward using the full dynamical model as

$$\tilde{\boldsymbol{x}}_2 = \boldsymbol{\varphi}(\tilde{\boldsymbol{x}}_1, t_1; t_2) \tag{14}$$

where $t_2 = t_1 + t_{12}$ and $\boldsymbol{\varphi}(\boldsymbol{x}_0, t_0; t_f)$ is the flow of Eq. (1) (written in the first-order canonical form) from initial state and time $(\boldsymbol{x}_0, t_0)$ to a final time t_f. Let $\tilde{\boldsymbol{x}}_2 = (\tilde{\boldsymbol{r}}_2, \tilde{\boldsymbol{v}}_2)^\top$. In general, $\tilde{\boldsymbol{r}}_2 \neq \boldsymbol{r}_2$, and this deviation is used

to compute the correction term $\delta\boldsymbol{v}_1$ for the initial velocity $\tilde{\boldsymbol{v}}_1$. The right-hand side of Eq. (14) can be expanded in first-order Taylor series about $\tilde{\boldsymbol{x}}_1$, i.e.,

$$\boldsymbol{\varphi}(\tilde{\boldsymbol{x}}_1 + \delta\boldsymbol{x}_1, t_1; t_2) \cong \boldsymbol{\varphi}(\tilde{\boldsymbol{x}}_1, t_1; t_2) + \boldsymbol{\Phi}(t_1, t_2)\delta\boldsymbol{x}_1 \tag{15}$$

where $\boldsymbol{\Phi}(t_0, t_f) := \partial\boldsymbol{\varphi}(\boldsymbol{x}_0, t_0; t_f)/\partial\boldsymbol{x}_0$ is the state transition matrix. By enforcing that the left-hand side of Eq. (15) is $(\boldsymbol{r}_2, \bar{\boldsymbol{v}}_2)^\top$, with $\bar{\boldsymbol{v}}_2$ unknown, and by using $\delta\boldsymbol{x}_1 = (\boldsymbol{0}, \delta\boldsymbol{v}_1)^\top$, one obtains

$$\delta\boldsymbol{v}_1 = \boldsymbol{\Phi}_{rv}^{-1}(t_1, t_2)(\boldsymbol{r}_2 - \tilde{\boldsymbol{r}}_2) \tag{16}$$

where $\boldsymbol{\Phi}_{rv}$ is the upper-right 3×3 block of $\boldsymbol{\Phi}$. Equation (16) allows computing the adjusted velocity as $\tilde{\boldsymbol{v}}_1^* = \tilde{\boldsymbol{v}}_1 + \delta\boldsymbol{v}_1$. The process is iterated until $\|\boldsymbol{r}_2 - \tilde{\boldsymbol{r}}_2\| < \varepsilon$, with ε a selected tolerance.

4 Waypoint trajectories

In this section we present qualitative and quantitative analyses, to assess the dynamical properties of trajectories in the *mid-range* region of Didymos system. Section 4.1 discusses the dynamics of single ballistic arcs, in terms of geometrical and dynamical properties. This drives the selection of waypoints and ballistic time of flight between consecutive maneuvers, as function of the distance from Didymos barycenter. This information is used to efficiently compute multi-arc loops, as shown in Section 4.2. All solutions are designed using the waypoint approach, considering ballistic arcs patched together at maneuvering points, and differ for the geometry of waypoints selected.

Arc-loop orbits are typically used to design trajectories that are permanently on the dayside of the asteroid. In this case, the waypoints are located between the Sun and Didymos system, and the spacecraft would see the asteroids illuminated at all time. This feature is desirable as it maximizes the opportunities for scientific observations of the asteroids, and moreover it is paramount when optical navigation is used. In the mid-range region around Didymos, it is important to consider the effect of the SRP, felt by the CubeSat as a constant push in the anti-Sun direction, towards the asteroid. In this context, the trajectory can be designed to leverage the effect of the SRP, which can be used to get closer to the asteroid.

4.1 Dynamics of ballistic arcs

Multi-arc loops can be constructed in a modular fashion, starting from a *fundamental* two-waypoint arcs. To select properly the waypoints, it is worth analyzing the geometrical and dynamical properties of several fundamental two-waypoints arcs. In particular, we investigate the geometrical positioning of waypoints and the properties of the ballistic arcs between them, in terms of distance from Didymos system, ballistic time of flight and relative distance between waypoints. To this goal, we study the properties of a single ballistic

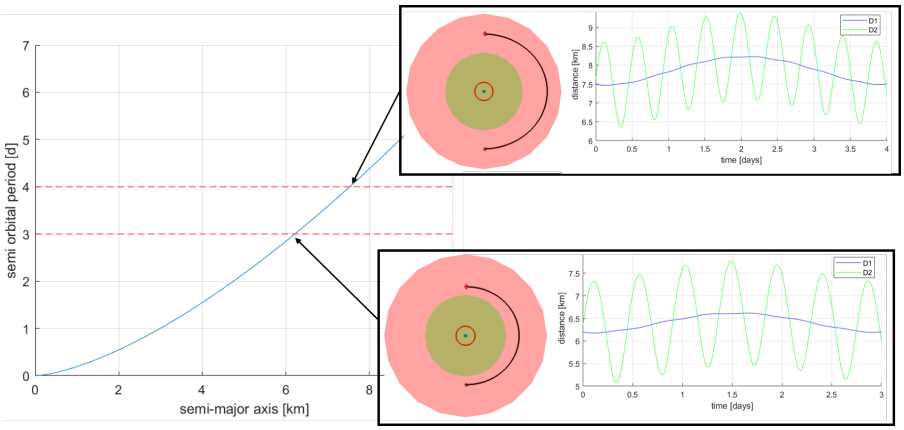

Fig. 7: Relation between semi-major axis and semi-orbital period for a purely Keplerian orbit around Didymos barycenter (left). Quasi-circular trajectories in the high-fidelity model of Didymos for the case of 3-day arc (lower-right) and 4-day arc (upper-right). Trajectories are shown in the equatorial plane of Didymos system, with Sun always to the right in the figures. The blue dot is Didymos (primary), while the orbit of Dimorphos is depicted in red. Green and red disks around Didymos are respectively at 5 km and 10 km distance from the barycenter of Didymos system (for reference). Ranges along the trajectory are shown with respect to D1 and D2 in the right part of the figure.

arc between two waypoints at -90 deg and +90 deg phase angles (CubeSat-Didymos barycenter-Sun angle).

First of all, we study the correlation between time of flight and distance from Didymos system. As a limiting case, we consider a quasi-circular arc (half of quasi-circular orbit around the Didymos system). We call them quasi-circular because they are computed in the high-fidelity dynamical model near Didymos, which includes the effect of SRP and thus they are not perfectly circular, as a purely Keplerian orbit would be. Apart from such dynamical perturbations, their range correspond roughly to the exact Keplerian solution reported in Figure 7 (left), which shows the time of flight (semi-orbital period of a R2BP orbit) as function of the distance from Didymos system (semi-major axis of a R2BP orbit). Alongside, we highlighted solutions in the high-fidelity model corresponding to a three- (lower-right) and four-day (upper-right) arc duration. Starting from the purely Keplerian motion, three-day quasi-circular arcs are found at about 6.2 km from Didymos and four-day quasi-circular arcs are found at about 7.5 km distance.

As expected, the analysis shows that shorter quasi-circular arcs and time of flights are required to fly closer to the system. We extend this to arcs with non-zero eccentricity. In particular, it is shown that the time of flight on a ballistic arc provides a strong limitation to the pericenter distance of the arc. In this case, we perform a parametric analysis by increasing the distance of waypoints,

but keeping the time of flight fixed. In particular, we start from the quasi-circular 3-day arc, and increase progressively the distance of waypoints. As expected, an increase of the distance between waypoints (with constant time of flight of three days) results in a higher velocity and energy/eccentricity of the orbit (from quasi-circular to quasi-elliptic, to quasi-hyperbolic). In terms of distance from Didymos system, we note a slight decrease of pericenter radius. However, this decrease is extremely small compared to the increase required in distance of waypoints, as shown in Figure 8. For instance, a pericenter distance of 3 km within a 3-day arc can be reached for a distance of 200 km between waypoints. For the case of motion within the mid-range region of Didymos (<10 km), the relation in Figure 7 applies roughly as a general case, and not only for quasi-circular arcs. In this region the time of flight is tightly connected to the minimum distance achievable, which cannot be lowered substantially by increasing the energy of the arc. As a result, two possibilities exist to fly lower-range arcs: a) reduce the ballistic time of flight between consecutive waypoints, or b) relax the hypothesis of flying within asteroids' dayside only. The first (a) implies a higher maneuver frequency and therefore more expensive strategy in terms of Δv cost and operational burden. The second (b) implies flying in the night-side of Didymos, which can be extremely challenging or even unfeasible when optical navigation is used.

Finally, we provide here a quantitative analysis on maneuvering cost. We consider simple two-waypoint/two-arc loops, made of one 4-day and one 3-day arc. As mentioned, these simple, fundamental loops are the building blocks of multi-arc loops shown in Section 4.2. In addition, we extend the parameter space to include a larger set of phase angles for waypoints, not limited to the ± 90 deg case. The deterministic Δv required to perform one fundamental loop can be precisely computed by evaluating the velocity discontinuity required at waypoints (two maneuvers at waypoints). We study here the effect of smaller to larger distance between waypoints. As expected, the higher the distance, the higher the velocity along the arc and the higher the eccentricity. Alongside with the velocity increase, the Δv is also expected to increase. We performed a parametric analysis to estimate the cost of several fundamental loops as function of their eccentricity. Figure 9 shows a summary of the parametric analysis. Note that each arc admits a range of eccentricity values. This is consistent with the dynamical environment: the ballistic arc is not a purely Keplerian solution and the variation of eccentricity is a direct effect of the SRP acceleration on the CubeSat. As expected, Figure 9 shows that the Δv cost increases with the eccentricity of the arc.

4.2 Multi-arc loop examples

Multi-arc loops are trajectories made of several discontinuous arcs arranged in a repetitive loop. This strategy has flight heritage and is now consolidated as baseline in many space exploration missions. It is the one currently envisaged by the Hera spacecraft during its operational phases and was previously used

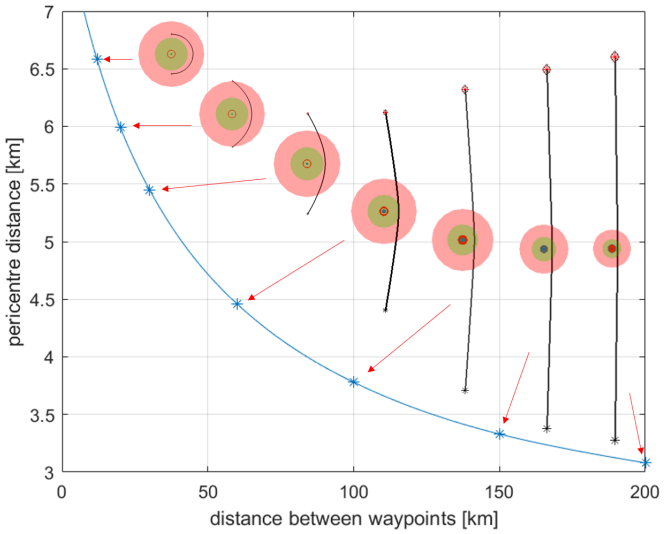

Fig. 8: Relation between pericenter distance and distance between waypoints (at -90 deg and +90 deg) for a 3-day arc in the high-fidelity Didymos model. Trajectories are shown in the equatorial plane of Didymos system, with Sun always to the right in the figures. The blue dot is Didymos (primary), while the orbit of Dimorphos is depicted in red. Green and red circles around Didymos are respectively at 5 km and 10 km distance from the barycenter of Didymos system (for reference).

by the Rosetta spacecraft during the science characterization phase around comet 67P/Churuymov-Gerasimenko (Accomazzo et al, 2015). As mentioned, the main advantage of this strategy is its high flexibility in terms of orbit geometry, which can be set to meet observational and operational requirements. Such flexibility can be achieved by accepting large variations in absolute value and direction of the velocity vector at maneuvering points. In principle, this comes at the cost of a higher Δv compared to stable orbits, because of plane changes after each maneuver. However, maneuvering cost is typically not critical for the case of low-gravity environment such as the proximity of small celestial bodies.

We provide here few examples, suitable to the Milani mission scenario (Ferrari et al, 2021). We consider sequences of arcs arranged in a weekly pattern. This is typical in terms of spacecraft operations, since it fits within a weekly schedule planning.

Figure 10 shows an example of a 6-waypoint hyperbolic loop strategy. The 6-waypoint loop is constructed in a 4-3-4-3-4-3 maneuvering pattern, with 4-day arcs followed by 3-day arcs, built by merging three consecutive 4-3 fundamental blocks. Each arc lies on a different orbital plane: the inclination of

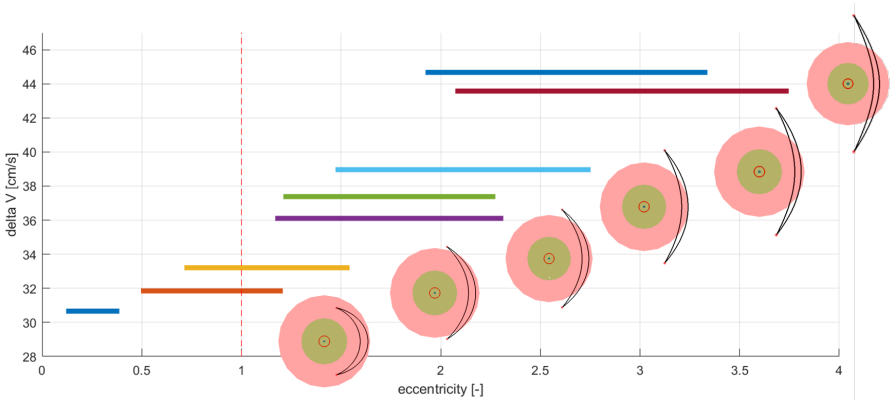

Fig. 9: Δv cost as function of the eccentricity range of the fundamental loop. Trajectories are shown in the equatorial plane of Didymos system, with Sun always to the right in the figures. The blue dot is Didymos (primary), while the orbit of Dimorphos is depicted in red. Green and red circles around Didymos are respectively at 5 km and 10 km distance from the barycenter of Didymos system (for reference).

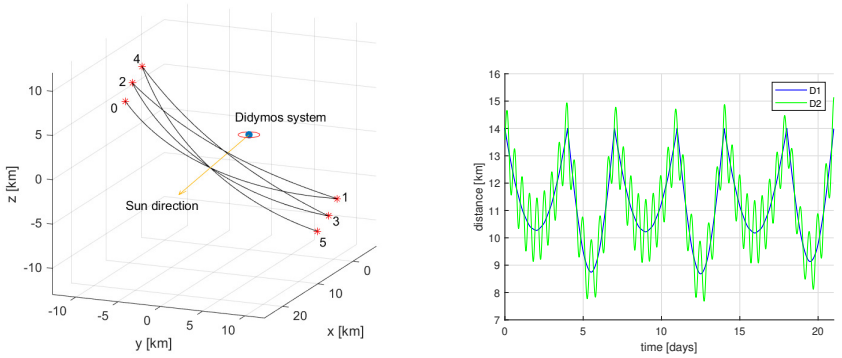

(a) (b)

Fig. 10: 6-waypoint loop on the day-side of Didymos system (4-3 maneuvering pattern). (a) Trajectory in the Didymos Equatorial reference frame, with Sun direction towards the positive x axis. (b) Range to Didymos primary (D1) and Dimorphos (D2) during the loop.

the plane changes with a rotation of 5 deg around the x-axis after each arc, as clearly visible in Figure 10a. This allows to observe the poles of D1 and D2, and to span different elevations above (and below) the equatorial plane of Didymos, covering similar latitudes with slightly different phase angles. Typically, this is a nice-to-have feature for imaging and scientific observations (Ferrari

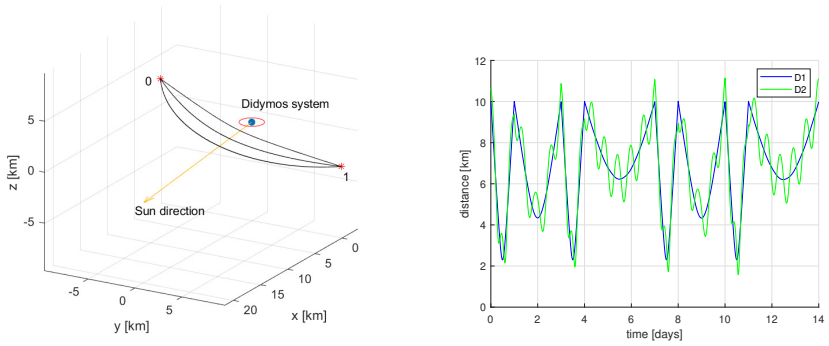

(a) (b)

Fig. 11: 2-waypoint loop on the day-side of Didymos system (1-2-1-3 maneuvering pattern). (a) Trajectory in the Didymos Equatorial reference frame, with Sun direction towards the positive x axis. (b) Distance to Didymos primary (D1) and Dimorphos (D2) during the loop.

et al, 2021). Figure 10b shows that 4-day arcs have pericenters above 10 km, while 3-day arcs flies below 9 km. In this case, the average maneuver cost to move between arcs is around 18 cm/s, and the whole loop sums up to a value of 0.920 m/s. The loop can be maintained at a cost of approximately 0.3 m/s/week. Note that these values are deterministic only and unmargined.

As further example, we show a 2-point hyperbolic loop strategy. Figure 11a shows the trajectory in the Didymos Equatorial reference frame. The loop has two waypoints only, but is constructed on four arcs on a 1-2-1-3 maneuvering pattern. All arcs lie on the same orbital plane, with nonzero inclination above the equatorial plane of Didymos system. This allows to observe the poles of D1 and D2. Figure 11b shows distances with respect to D1 and D2 during the whole loop. 1-day arcs have pericenter of about 2 km, 2-day arcs flies just above 4 km and 3-day arcs have pericenter above 6 km. Due to a shorter distance from Didymos system, the average maneuver cost between arcs increases with respect to the previous example and is around 32 cm/s, while the whole loop sums up to a value of 2.179 m/s. The loop can be maintained at a cost of approximately 1 m/s/week. Note that these values are deterministic only and unmargined.

5 Conclusion

The paper provides a general description of the dynamical environment near Didymos binary system and presents suitable trajectory options for a CubeSat flying in the dayside of the asteroids. As case study, we focus on the Hera Milani CubeSat mission scenario.

The dynamical environment is subdivided into three main regions, identified by different dynamical regimes. We provide a detailed analysis of the dynamical effects acting on the CubeSat and their relevance in each region, by comparing the acceleration field computed using several dynamical models. The *inner* region is approximately delimited by the orbital radius of Dimorphos. In this region, the gravity of the asteroids is predominant and high-fidelity models of their mass distribution are required to accurately reproduce the dynamical environment. The dynamics in this region are extremely chaotic and sensitive to uncertainties. The *mid-range* region is identified between 1.3 and 10 km from Didymos barycenter. In this region the effects due to the gravity of the asteroid system and the SRP are commensurate and equally important. The *outer* region extends beyond 10 km. This is largely dominated by SRP and, farther away, by the third-body effect of the Sun. We identify the *mid-range* region as a suitable region to host the scientific operations of a CubeSat. This provides a good balance between the scientific benefits of flying close to the asteroid system and the operational benefits of flying a CubeSat in a region with less-chaotic dynamics, more robust to uncertainties. We investigate suitable trajectories flying entirely in the dayside of the asteroids using a flexible waypoint approach. In this context, the deterministic Δv cost of CubeSat maneuvers is estimated in the order of 0.3-1 m/s/week, with a maneuver frequency between 1 to 4 days.

Acknowledgements This work has been performed in response to ESA call AO/1-10258/20/NL/GLC: Hera Mission "Second CubeSat" Phase A/B C/D & E1. FF acknowledge funding from the European Union's Horizon 2020 research and innovation programme under the Marie Skłodowska-Curie grant agreement No. 800060. MP and FT acknowledge funding from the European Union's Horizon 2020 research and innovation programme under the Marie Skłodowska-Curie grant agreement No. 813644. The authors would like to acknowledge the support received by the whole Milani Team.

Conflict of interest The authors state that there is no conflict of interest.

References

Accomazzo A, Ferri P, Lodiot S, Pellon-Bailon JL, Hubault A, Porta R, Urbanek J, Kay R, Eiblmaier M, Francisco T (2015) Rosetta operations at the comet. Acta Astronautica 115:434–441, DOI 10.1016/j.actaastro.2015.06.009

Agrusa HF, Richardson DC, Davis AB, Fahnestock E, Hirabayashi M, Chabot NL, Cheng AF, Rivkin AS, Michel P (2020) A benchmarking and sensitivity study of the full two-body gravitational dynamics of the dart mission target, binary asteroid 65803 didymos. Icarus p 113849, DOI 10.1016/j.icarus.2020.113849

Capannolo A, Ferrari F, Lavagna M (2019) Families of bounded orbits near binary asteroid 65803 didymos. Journal of Guidance, Control, and Dynamics 42(1):189–198, DOI 10.2514/1.G003437

Cheng A, Atchison J, Kantsiper B, Rivkin A, Stickle A, Reed C, Galvez A, Carnelli I, Michel P, Ulamec S (2015) Asteroid impact and deflection assessment mission. Acta Astronautica 115(Supplement C):262 – 269, DOI 10.1016/j.actaastro.2015.05.021

Cheng AF, Rivkin AS, Michel P, Atchison J, Barnouin O, Benner L, Chabot NL, Ernst C, Fahnestock EG, Kueppers M, Pravec P, Rainey E, Richardson DC, Stickle AM, Thomas C (2018) AIDA DART asteroid deflection test: Planetary defense and science objectives. Planetary and Space Science 157:104–115, DOI 10.1016/j.pss.2018.02.015

Cheng AF, Stickle AM, Fahnestock EG, Dotto E, Corte VD, Chabot NL, Rivkin AS (2020) DART mission determination of momentum transfer: Model of ejecta plume observations. Icarus 352:113,989, DOI 10.1016/j.icarus.2020.113989

Chobotov VA (1991) Orbital Mechanics. AIAA Education Series

Damme F, Hussmann H, Oberst J (2017) Spacecraft orbit lifetime within two binary near-earth asteroid systems. Planetary and Space Science 146:1–9, DOI 10.1016/j.pss.2017.07.018

Davis AB, Scheeres DJ (2020) High-fidelity modeling of rotationally fissioned asteroids. The Planetary Science Journal 1(1):25, DOI 10.3847/psj/ab9a39

Dell'Elce L, Baresi N, Naidu S, Benner L, Scheeres D (2017) Numerical investigation of the dynamical environment of 65803 didymos. Advances in Space Research 59(5):1304–1320, DOI 10.1016/j.asr.2016.12.018

Ferrari F, Lavagna M (2018) Ballistic landing design on binary asteroids: The aim case study. Advances in Space Research 62(8):2245 – 2260, DOI 10.1016/j.asr.2017.11.033, past, Present and Future of Small Body Science and Exploration

Ferrari F, Lavagna M, Howell KC (2016) Dynamical model of binary asteroid systems through patched three-body problems. Celestial Mechanics and Dynamical Astronomy 125(4):413–433, DOI 10.1007/s10569-016-9688-x, URL http://dx.doi.org/10.1007/s10569-016-9688-x

Ferrari F, Franzese V, Pugliatti M, Giordano C, Topputo F (2021) Preliminary mission profile of hera's milani CubeSat. Advances in Space Research 67(6):2010–2029, DOI 10.1016/j.asr.2020.12.034

Goldberg HR, Karatekin O, Ritter B, Herique A, Tortora P, Prioroc C, Garcia Gutierrez B, Martino P, Carnelli I (2019) The juventas cubesat in support of esa's hera mission to the asteroid didymos. In: Small Satellite Conference

Guzzetti D, Sood R, Chappaz L, Baoyin H (2019) Stationkeeping analysis for solar sailing the l4 region of binary asteroid systems. Journal of Guidance, Control, and Dynamics 42(6):1306–1318, DOI 10.2514/1.g003994

Hou X, Scheeres DJ, Xin X (2016) Mutual potential between two rigid bodies with arbitrary shapes and mass distributions. Celestial Mechanics and Dynamical Astronomy 127(3):369–395, DOI 10.1007/s10569-016-9731-y

Jean I, Misra AK, Ng A (2019) Solar radiation pressure–compatible trajectories in the vicinity of a binary asteroid. Journal of Guidance, Control, and Dynamics 42(6):1319–1329, DOI 10.2514/1.g004007

Karatekin O, Goldberg H, Prioroc CL, Villa V, team J (2019) Juventas: Exploration of a binary asteroid system with a cubesat. In: Proceedings of the International Astronautical Congress, vol 2019-October

Kohout T, Näsilä A, Tikka T, Granvik M, Kestilä A, Penttilä A, Kuhno J, Muinonen K, Viherkanto K, Kallio E (2018) Feasibility of asteroid exploration using cubesats—aspect case study. Advances in Space Research 62(8):2239 – 2244, DOI 10.1016/j.asr.2017.07.036

Lasagni Manghi R, Modenini D, Zannoni M, Tortora P (2018) Preliminary orbital analysis for a cubesat mission to the didymos binary asteroid system. Advances in Space Research 62(8):2290 – 2305, DOI 10.1016/j.asr.2017.12.014, past, Present and Future of Small Body Science and Exploration

Michel P, Kueppers M, Sierks H, Carnelli I, Cheng AF, Mellab K, Granvik M, Kestilä A, Kohout T, Muinonen K, Näsilä A, Penttila A, Tikka T, Tortora P, Ciarletti V, Hérique A, Murdoch N, Asphaug E, Rivkin A, Barnouin O, Bagatin AC, Pravec P, Richardson DC, Schwartz SR, Tsiganis K, Ulamec S, Karatekin O (2018) European component of the AIDA mission to a binary asteroid: Characterization and interpretation of the impact of the DART mission. Advances in Space Research 62(8):2261–2272, DOI 10.1016/j.asr.2017.12.020

Naidu S, Benner L, Brozovic M, Nolan M, Ostro S, Margot J, Giorgini J, Hirabayashi T, Scheeres D, Pravec P, Scheirich P, Magri C, Jao J (2020) Radar observations and a physical model of binary near-earth asteroid 65803 didymos, target of the dart mission. Icarus p 113777, DOI 10.1016/j.icarus.2020.113777

Perez F, Modenini D, Vázquez A, Aguado F, Tubío R, Dolgos G, Tortora P, Gonzalez A, Manghi RL, Zannoni M, Nazeeruddin A, Melozzi M, Carnelli I (2018) DustCube, a nanosatellite mission to binary asteroid 65803 didymos as part of the ESA AIM mission. Advances in Space Research 62(12):3335–3356, DOI 10.1016/j.asr.2018.06.019

Scheeres DJ (1994) Dynamics about uniformly rotating triaxial ellipsoids: Applications to asteroids. Icarus 110(2):225–238, DOI 10.1006/icar.1994.1118

Scheeres DJ (2016) Orbital Motion in Strongly Perturbed Environments. Springer-Verlag GmbH

Scheirich P, Pravec P (2009) Modeling of lightcurves of binary asteroids. Icarus 200(2):531–547, DOI 10.1016/j.icarus.2008.12.001

Soldini S, Takanao S, Ikeda H, Wada K, Yuichi T, Hirata N, Hirata N (2020) A generalised methodology for analytic construction of 1:1 resonances around irregular bodies: Application to the asteroid ryugu's ejecta dynamics. Planetary and Space Science 180:104,740, DOI 10.1016/j.pss.2019.104740

Tardivel S (2016) Optimization of the ballistic deployment to the secondary of a binary asteroid. Journal of Guidance, Control, and Dynamics 39(12):2790–2798, DOI 10.2514/1.g000593

Tortora P, Tana VD (2019) LICIACube, the italian witness of DART impact on didymos. In: 2019 IEEE 5th International Workshop on Metrology for AeroSpace (MetroAeroSpace), IEEE, pp 314–317, DOI

10.1109/metroaerospace.2019.8869672
Van Wal S, Tardivel S, Scheeres D (2017) Parametric study of ballistic lander deployment to small bodies. Journal of Spacecraft and Rockets 54(6):1330–1355, DOI 10.2514/1.a33832
Villegas-Pinto D, Soldini S, Tsuda Y, Heiligers J (2020) Temporary capture of asteroid ejecta into periodic orbits: Application to JAXA's hayabusa2 impact event. In: AIAA Scitech 2020 Forum, American Institute of Aeronautics and Astronautics, DOI 10.2514/6.2020-0221
Werner RA (1994) The gravitational potential of a homogeneous polyhedron or don't cut corners. Celestial Mechanics & Dynamical Astronomy 59(3):253–278, DOI 10.1007/bf00692875
Werner RA, Scheeres DJ (1997) Exterior gravitation of a polyhedron derived and compared with harmonic and mascon gravitation representations of asteroid 4769 castalia. Celestial Mechanics and Dynamical Astronomy 65(3):313–344, DOI 10.1007/bf00053511
Yu Y, Michel P (2018) Ejecta cloud from the AIDA space project kinetic impact on the secondary of a binary asteroid: II. fates and evolutionary dependencies. Icarus 312:128–144, DOI 10.1016/j.icarus.2018.04.017
Yu Y, Cheng B, Hayabayashi M, Michel P, Baoyin H (2019) A finite element method for computational full two-body problem: I. the mutual potential and derivatives over bilinear tetrahedron elements. Celestial Mechanics and Dynamical Astronomy 131(11), DOI 10.1007/s10569-019-9930-4
Zannoni M, Tommei G, Modenini D, Tortora P, Mackenzie R, Scoubeau M, Herfort U, Carnelli I (2018) Radio science investigations with the asteroid impact mission. Advances in Space Research 62(8):2273–2289, DOI 10.1016/j.asr.2017.12.003